Hydroxamate titanium-organic frameworks and the effect of siderophore-type linkers over their photocatalytic activity

Natalia M. Padial,[†,⊥,‡] Javier Castells-Gil,[†,‡] Neyvis Almora-Barrios,[†] María Romero-Angel,[†] Iván da Silva,[∇] Mariam Barawi,[§] Alba García,[§] Víctor A. de la Peña O'Shea[§] and Carlos Martí-Gastaldo*,[†]

[†]Universidad de Valencia (ICMol), Catedrático José Beltrán-2, 46980, Paterna (Spain).

[∇]ISIS Facility, Rutherford Appleton Laboratory, Chilton, Didcot, Oxfordshire, OX11 0QX (United Kingdom).

[§]IMDEA Energy Institute, Parque Tecnológico de Móstoles, Avda. Ramón de la Sagra, 3, 28935 Móstoles, Madrid (Spain).

The chemistry of Metal-Organic Frameworks (MOFs) relies on the controlled linking of organic molecules and inorganic secondary building units to assemble an unlimited number of reticular frameworks. However, the design of porous solids with chemical stability remains still limited to carboxylate or azolate groups. There is a timely opportunity to develop new synthetic platforms that make use of unexplored metal binding groups to produce metal-linker joints with hydrolytic stability. Living organisms use siderophores (*iron carriers* in greek) to effectively assimilate iron in soluble form. These compounds make use of hard oxodonors as hydroxamate or catecholate groups to coordinate metal Lewis acids like iron, aluminium or titanium to form metal complexes very stable in water. Inspired by the chemistry of these microorganisms, we report the first hydroxamate

MOF prepared by direct synthesis. MUV-11 (MUV = Materials of Universidad de Valencia) is a crystalline, porous material (close to 800 $m^2 \cdot g^{-1}$) that combines photo-activity with outstanding chemical stability in acid conditions. By using a high-throughput approach, we also demonstrate that this new chemistry is compatible with the formation of single crystalline phases for multiple titanium salts, thus expanding the scope of precursors accessible. Titanium frameworks are regarded as promising materials for photocatalytic applications. Our photoelectrochemical and catalytic tests suggests important differences for MUV-11. Compared to other Ti-MOFs, changes in the photoelectrochemical and photocatalytic activity have been rationalized with computational modelling revealing how the chemistry of siderophores can introduce changes to the electronic structure of the frontier orbitals, relevant to the photocatalytic activity of these solids.
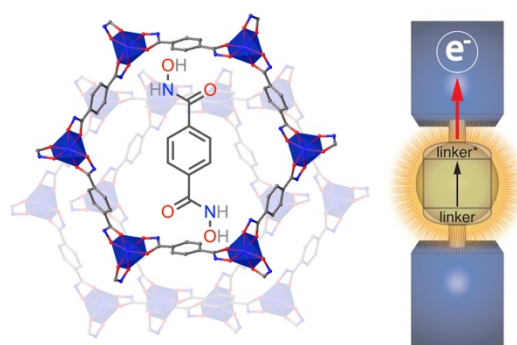
INTRODUCTION

Metal-Organic Frameworks (MOFs) are crystalline porous materials built from the interlinking of metal nodes and organic linkers. Their unparalleled chemical and structural flexibility provides a rich landscape of pore environments and physical properties of interest in gas storage/separation, catalysis, sensing or proton transport to cite a few.[1] MOFs based on divalent transition metal ions have led to numerous open architectures with increasingly high porosity. However, they often suffer from poor chemical stability, in particular to water, thus limiting their application. This problem can be circumvented by introducing strong metal-linker coordination bonds less prone to hydrolysis either by reaction of soft azolate

linkers with divalent metals, i.e. ZIF and pyrazolate families,[2,3] or by combination of hard carboxylates with highly charged metals (M^{3+} and M^{4+}). This last approach was first exemplified for Al^{3+}, Fe^{3+} and Cr^{3+} in the MIL-53,[4] MIL-100[5] and MIL-101[6] families, followed by the discovery of the UiO-66 MOFs based on $Zr_6O_4(OH)_4(RCO_2)_{12}$ clusters as SBUs in 2008.[7] This accelerated the discovery of a high number of materials based on isostructural Zr^{4+} or Hf^{4+} metal-oxo clusters,[8,9] for a substantial increase in the number of stable MOFs reported in the last years.[10,11]

Compared to these metals, titanium is relatively low-cost, less toxic, redox active and displays photo-catalytic properties. Notwithstanding these advantageous features, the synthesis of Ti^{4+} crystalline, open frameworks remains still very challenging likely due to the high reactivity of the
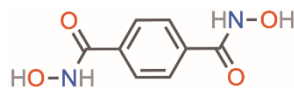
Scheme 1. Structure of benzene-1,4-dihydroxamic acid (H_4bdha).

titanium sources employed. Common precursors are prone to hydrolysis in the solvothermal conditions used in MOFs synthesis, which often leads to uncontrolled precipitation of amorphous oxides or hydroxides.[12] As a result, only a few porous Ti-MOFs have been prepared by direct reaction with polycarboxylate linkers.[13–22] Unfortunately, we are still far from being capable of rationalising the design of new topologies arguably due to the arbitrary polycondensation reactions of Ti cations in solution, that limit our control over the nuclearity of the metal-oxo clusters that will be incorporated into the framework. An interesting perspective in this context is the use of alternative linkers that allow for certain control over this equilibrium, based on strong complexation of the metal to direct the formation of foreseeable framework nodes. This is the case of Ti-CAT-5,[23] NTU-9[24] and MIL-167,[25] in which the replacement of carboxylates with chelating catecholate or phenolate groups favours the formation of mononuclear Ti nodes with octahedral coordination. Still, porosity in these solids can be severely limited by structural interpenetration or the presence of cations for charge neutrality.

These precedents encouraged us to investigate the use of siderophore-type linkers by replacing carboxylate with hydroxamic units (-CONHOH) into already known MOF-forming polycarboxylate linkers. Compared to carboxylates, hydroxamates are well-known for their medical applications and ability to form strong metal-linker joints.[26] Still, there is no precedent for their use as connectors to form porous, crystalline materials by direct synthesis. This is arguably due to the difficulties in controlling the formation of strong metal-hydroxamate coordination bonds under reversible conditions to avoid the formation of amorphous materials with intrinsic disorder. To date, hydroxamic acid linkers have been only incorporated post-synthetically into Zr(IV)-UiO-66 frameworks via solvent-assisted linker exchange reactions to produce daughter materials with enhanced stability.[27] Herein, we report the first hydroxamate-based MOF prepared by *de novo* synthesis. MUV-11 (MUV = Materials of Universidad de Valencia) is a crystalline, porous materials that combines photo-activity with a surface area close to 800 m²·g⁻¹. Compared to titanium frameworks based on other binding groups, the use of a siderophore binder results in outstanding chemical stability in acid conditions and introduces drastic changes to the frontier crystalline orbitals that control charge transfer kinetics and thereby the photocatalytic activity of this material.

RESULTS AND DISCUSSION

Synthesis and structure of MUV-11. Benzene-1,4-dihydroxamic acid (H_4bdha) can be prepared by one-step reaction of the ester derivative of terephthalic acid with a methanolic solution of hydroxylamine under basic conditions.[28] This reaction is well fitted for multigram-scale linker synthesis as it proceeds with yields close to 65% (**S2**). MUV-11 was first prepared by solvothermal reaction of H_4bdha with titanium (IV) isopropoxide in dry *N,N*-dimethylformamide (DMF) at 120 °C by using acetic acid as
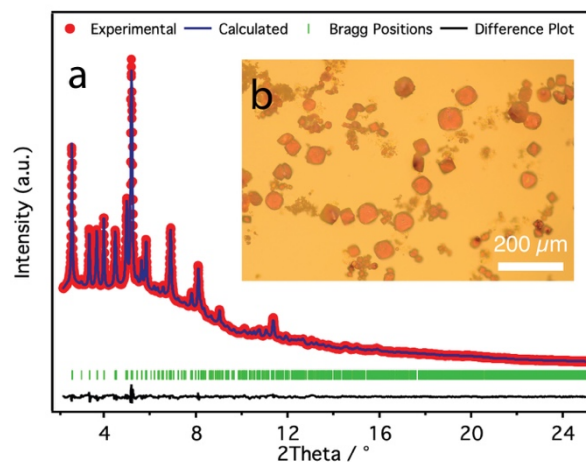

Figure 1. a) Rietveld refinement of MUV-11 crystals (λ = 0.413070(1) Å). b) Size and morphology of the crystals formed.

modulator. The product can be quantitatively formed either in capped vials, Teflon liners or easily adapted to high-scale synthesis by using glass bottles (See experimental section for synthetic details). Reagents manipulation was carried out in the glove box to avoid partial hydrolysis of the titanium precursor.

The solid was isolated as orange crystals with hexagonal morphology and sizes ranging from 10 to 20 μm (**Figures 1b** and **S3**). Their small size and intertwined nature prevented structural determination with an in-house diffractometer. Synchrotron radiation (ALBA, BL13-XALOC) was limited by very weak diffraction at high-angle resolution and only allowed us to determine the space group and cell parameters. Electron density maps were used to determine the position of Ti atoms, organic linkers and the overall network connectivity. This preliminary structural model was then modified with the Materials Studio (MS) 2017 R2 and optimized with DFT methods (**S4**) to produce a starting model for the refinement of the high-resolution powder X-Ray diffraction data (PXRD) also collected at the synchrotron (ALBA, BL04-MSPD). As shown in **Figure 1a**, Rietveld refinement converged with excellent residual values (Rwp = 1.47%, Rexp= 1.15%) for a trigonal P3₂ space group with cell parameters a = 18.1230(8) Å, c = 11.2238(7) Å. Comparison of the atomic coordinates generated by DFT and Rietveld refinement are summarised in **Tables S5** and **S6**. MUV-11 is based on octahedrally coordinated, single-node Ti(IV) atoms. They are coordinated to six oxygen atoms from the hydroxamic groups of three $H_n$bdha (n = 1, 2) units that interconnect two neighbouring metal nodes. This conforms a honeycomb-like lattice in which simple-node metal atoms and organic linker act as vertices and edges of the hexagonal tiling for a 2,3-c 2-nodal net topology (**Figure 2a** and **S15**). This is reminiscent of the in-plane structure of NTU-9,[24] built from 2,5-dihydroxiterephthalate (H_2dhtp) linkers, with 1.5 times bigger pore widows result of the elongation of the linker in MUV-11 (**Figure S14**). The hydroxamic group is capable of adapting the coordination mode of dhtp connectors into a 5-membered chelate, but it introduces differences that result in important changes to the internal structure of the layers. As summarised in Figure **S16**, the -OH groups in dhtp form part of the
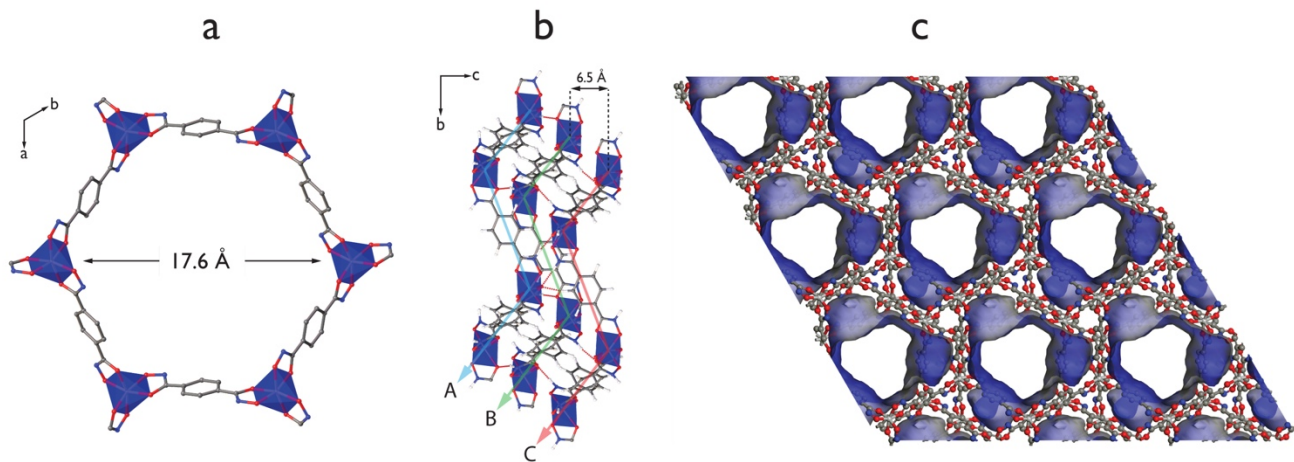
Figure 2. a) Honeycomb lattice in MUV-11 showing the internal dimensions of the pore window in the layer. b) ...ABC... packing of the weavy layers [Ti$_2$(Hbdha)$_2$(H$_2$bdha)] directed by the interlayer H-bonds. c) Perspective of MUV-11 along the c axis showing the Connolly representation of the 1D channels with triangular shape responsible for the porosity in the solid (Pale blue, 1.2 Å probe radius). Hydrogen atoms and solvent molecules have been omitted for clarity.

central aromatic ring, restricting the linker to adopt a planar conformation upon metal coordination with a twist angle between neighbouring rings of 4.4° in NTU-9. In turn, the hydroxamate group lies off the ring and can rotate more freely to adopt the conformation more favourable energetically. As a result, the planes of the aromatic ring and one of the Ti-OCNO chelates deviate 16.3° from planarity to produce highly distorted octahedron. This is likely the reason for the layers in MUV-11 to adopt a zigzag configuration (**Figure 2b**) compared to their planar structure in NTU-9. The internal rotation of the hydroxamate units is also influenced by the formation of NH···O H-bonds between neighbouring layers of 2.74(14) and 2.73(11) Å (**Figure S17** and **Table S7**). We presume the corrugated structure of the layers and H-bond interactions are responsible for the packing of the solid. Compared to NTU-9, that displays an ...AA... eclipsed packing, MUV-11 combine three types of neutral [Ti$_2$(Hbdha)$_2$(H$_2$bdha)] layers arranged in a ...ABC... fashion for an overall slipped packing. As shown in **Figure 2c**, this results in the formation of empty 1D channels along [001] with a pseudo-hexagonal shape and internal diameter of 0.8 nm, that account for a solvent-accessible volume close to 40 % (**Table S8**) and a theoretical surface area near 950 m^2·g^{-1} as estimated with Zeo++.[28]

High-throughput screening of other metal precursors. Possibly one of the most important requirements to access crystalline Ti-MOFs is to gain control over the hydrolytic stability of the metal precursor under framework forming conditions to prevent the formation of amorphous titanium oxide. Asides the use of pre-formed clusters,[14,16,18,22] this is arguably the reason for which most materials have been produced by using primarily titanium(IV) isopropoxide (TTIP), i.e. MIL-177,[19] MIL-168,169,[25] MIL-125,[13] Ti-CAT-5,[23] MOF-902,[16] NTU-9[29] or MUV-10[20] and bis(cyclopentadienyl)titanium (IV) dichloride (BCTTD) for COK-69.[30] Enlarging the pool of precursors compatible with solvothermal synthesis might help accelerating the discovery of new titanium-organic frameworks. This pushed us to investigate the synthesis of MUV-11 by using other affordable Ti salts with variable reactivity in water. Accordingly, we replaced TTIP in the

original synthesis with other six precursors including BCTTD, cyclopentadienyltitanium(IV) trichloride (CTTT), titanium (IV) n-propoxide (TTP), titanium (IV) n-butoxide (TTB), titanium (IV) 2-ethylhexyloxide (TTEEO) and titanium (IV) triethanolaminato)isopropoxide (TTTEI), (**Table S1**).

3

We used a FLEX SHAKE high-throughput workstation from Chemspeed© for robotic dispensing of solids and liquids in order to accelerate the screening and systematic study of the multiple variables in play (temperature, reaction time, solvent, concentration and modulator) to define the best set of conditions for the synthesis of crystalline MUV-11 regardless the precursor, whilst ensuring reproducibility. See **S3** for a detailed description of all the variations explored. Our experiments confirm that phase pure MUV-11 can be also prepared from TTP, TTB and TTTEI with yields between 50-70%. The use of TTEEO and organometallic precursors (BCTTD and CTTT) yielded amorphous phases in all cases. We used Scanning Electron Microscopy (SEM) and PXRD to evaluate the effect of the precursor over the particle size and crystallinity of the material (**Figure 3**). All solids crystallise as lamellae particles with hexagonal morphology. Their average size increases from 5 to 50 μm according to the sequence TTP < TTIP < TTB < TTTEI. This last precursor also drives the formation of the most crystalline MUV-11 phase. Just like for sol-gel processing, our results suggest that the modification of the titanium alkoxide with multidentate -$(OC_4H_4)_3N$ linkers in TTTEI help controlling its reactivity in presence of water.[31] This chelate is less readily hydrolysed than -OR groups in the conditions required for the crystallization of the framework, thus preventing the rapid formation of amorphous materials.

Porosity and chemical stability. The best product in terms of yield, homogeneity and crystal size was obtained by using TTTEI. As summarised in **S5**, phase purity of the batch was confirmed by CHN analysis, SEM, LeBail refinement of the powder X-ray diffraction and thermogravimetric analysis (TGA). Based on CHN we determine a unit formula of $[Ti_2(Hbdha)_2(H_2bdha)]\cdot(DMF)_{0.5}\cdot(H_2O)_{3.3}$ for the as-made solid. TGA of the desolvated material is consistent with the 23.1% of residual TiO_2 formed (Calc. 23.6%). MUV-11 displays a thermal stability similar to other Ti-MOFs. As expected from the formation of thermodynamically strong Ti-O coordination bonds, complete decomposition takes place above 400 °C. However, there is significant mass loss at 240 °C that might be linked to the partial decomposition of bdha units, more prone to oxidation than carboxylate linkers (**Figure S20**).

Porosity was studied by N_2 adsorption-desorption isotherms at 77 K. after exchanging the as-made solid with acetone, followed by activation at 100 °C (10^{-3} mbar). MUV-11 displays a reversible type-I N_2 adsorption characteristic of microporous materials, with a small hysteresis above $P/P_0 = 0.4$ indicative of intergrain mesoporosity (**Figure 4a and S23**). The multi-point BET surface area was found to be 756 $m^2 \cdot g^{-1}$. Analysis of the pore size distribution (PSD) by using non-linear density functional theory (NLDFT) methods reveals a homogeneous pore diameter of 1.0 nm, that agrees well the 0.8 nm calculated from the structure. We also confirmed the porosity of the solid with CO_2. MUV-11 displays a reversible type-I isotherm at 195 K with less abrupt adsorption at low pressures (**Figure S25**). At high temperatures, it displays a modest gravimetric uptake of 1.23 $mmol \cdot g^{-1}$ of CO_2 at 293 K and 1 bar (5.4 wt%), with an isosteric heat of adsorption of 29.9 $kJ \cdot mol^{-1}$ (**Figure S26**). Similar to the introduction of amino groups, replacement of carboxylic groups with nitrogenated hydroxamate -$CONHO^-$ units seems responsible for more favourable interaction of CO_2 molecules
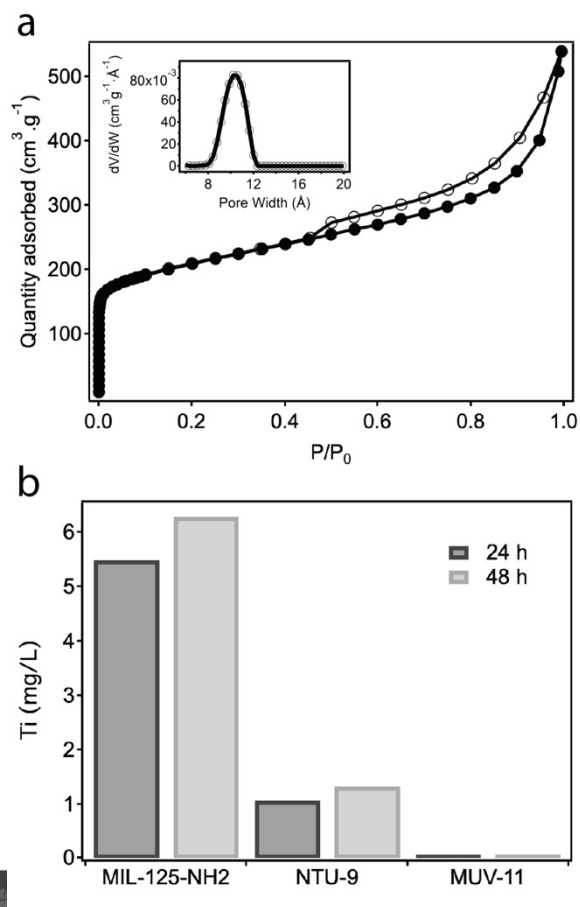

Figure 4. a) N_2 adsorption at 77 K of MUV-11 exchanged with acetone. Inset shows the experimental PSD. b) ICP-MS measurements of MIL-125-NH$_2$, NTU-9 and MUV-11 at pH 2 after 24 and 48 hours.
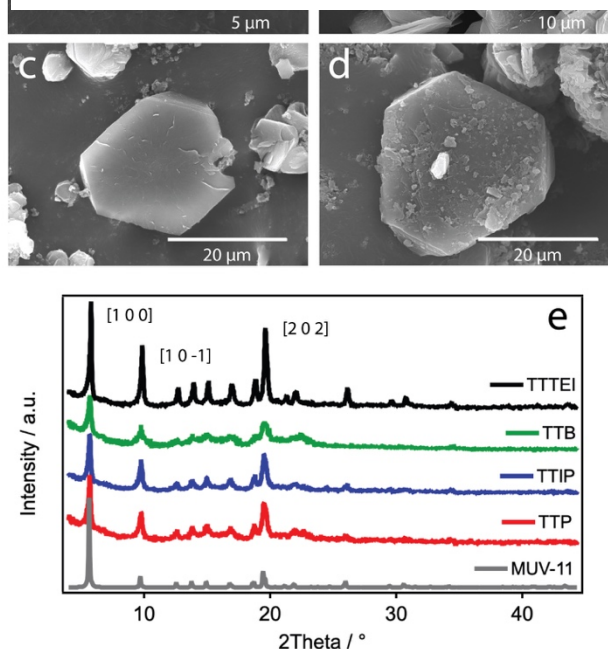

Figure 3. Effect of the Ti(IV) precursor used in the synthesis of MUV-11 over the morphology and size of the particles formed: a) TTP, b) TTIP c) TTB, d) TTTEI and e) changes to the crystallinity of the framework.

with the surface of the pores. It is worth noting that the structure of MUV-11 is quite sensitive to the activation protocol employed. Soxhlet washing of the solid with protic solvents lead to partial collapse of the structure for a substantial reduction of accessible porosity (**Figure S24**). This is likely due to the network of H-bonds that direct interlayer packing and thereby dictate the 3D structure of MUV-11 (**Figure 2b**). Compared with solvents like acetone, not capable of H-bonding, solvent exchange with methanol result in partial amorphization likely due to a disordered reorganization of interlayer interactions.

We evaluated the chemical stability of MUV-11 after immersion of the solid for during hours in concentrated solutions of HCl and NaOH(aq) between pH 1 and 14. The PXRD of the solids recovered confirm retention the diffraction lines characteristic of the solid together with a partial amorphization of the framework, likely linked to the distortion of interlayer packing interactions by interaction with water (**S6**). We also investigated the effect of hydroxamic connectors over the chemical stability of MUV-11 in comparison to other Ti-MOFs based on carboxylate linkers like terephthalic acid (MIL-125-NH$_2$) and dhtp (NTU-9). ICP-MS analysis of the supernatants of the solids after incubation at pH 2 for 24 and 48 hours shows negligible metal leaching for MUV-11 (**Figure 4b**). In turn, the concentration of titanium in solution increases with time up to a maximum of 6.3 and 1.3 mg·mL^{-1} for MIL-125-NH$_2$ and NTU-9, respectively, after 48 hours (**Table S9**). We presume that the differences in the degradation rates of the solids are controlled by the changes in the stability constants for complex formation, higher for dhtp and bdha as result of the formation of five-membered chelates. Anionic hydroxamates are known to form hard oxodonors that bind strongly to Lewis acids, resulting in complexes with remarkably high stability constants.[32] Our results confirm that this strong metal joints are capable of preventing chemical degradation to endow MUV-11 with outstanding stability in acid medium. It is instead the structural flexibility intrinsic to the interlayer packing in the solid, which directs structural changes for the collapse of this particular framework.

Electronic structure and photoelectrochemical response. The use of Ti-MOFs as photocatalysts for solar fuel production or light-induced organic transformations is gaining importance due to the combination of high surface areas and chemical stability with the redox versatility and photoactivity intrinsic to titanium.[33] As shown in **Figure 5a**, the Tauc Plot obtained through the diffuse reflectance spectra of MUV-11 confirms a broad absorption in the visible region from 300 to 550±10 nm. An optical band gap energy of 2.01±0.01 eV was calculated through the Kubelka-Munk function. This value is smaller than those reported for COK-69 (3.77 eV), MIL-125 (3.6 eV), MUV-10(Ca) (3.1 eV), MOF-901 (2.65 eV), MIL-125-NH$_2$ (2.6 eV) whilst slightly above PCN-22 (1.93 eV) and NTU-9 (1.72 eV).

For a clearer understanding of the electronic structure of MUV-11 we prepared electrodes by drop casting a suspension of the MOF on ITO cover glasses (See experimental section). Electrochemical impedance spectroscopy (EIS) and cyclic voltammetry (CV) measurements were used to estimate the flat band potential and determine the absolute positions of the valence and conduction band edges in MUV-11 (**Figures 5a, b**). The Mott-Schotky plot confirms that MUV-11 displays *p*-type conductivity with a flat-band potential of 0.68±0.02 V *vs.* Ag/AgCl or 0.48±0.02 V vs the normal hydrogen electrode (NHE). The CV of MUV-11 films in a nonaqueous electrolyte (0.1M NBu$_4$PF$_6$ in acetonitrile) shows the presence of anodic and cathodic peaks at -0.8 and 1.6 V *vs* Ag/Ag$^+$ which was later corrected with the ferrocene couple. This experimental information was used to calculate the approximate positions of the HOMO and LUMO energies at -6.1 and -3.6 ± 0.1 eV. **Figure 5c** shows the comparison of the absolute energies of the HOMO, LUMO in MUV-11 with TiO$_2$ and the redox pairs for the hydrogen evolution reaction (HER, H$_2$O/H$_2$) and oxygen evolution reaction (OER, O$_2$/H$_2$O) at pH = 0. The LUMO is higher in energy than H$_2$O/H$_2$ and the HOMO is lower than O$_2$/H$_2$O in acid conditions, for which the MOF displays outstanding chemical stability. This suggests that, in
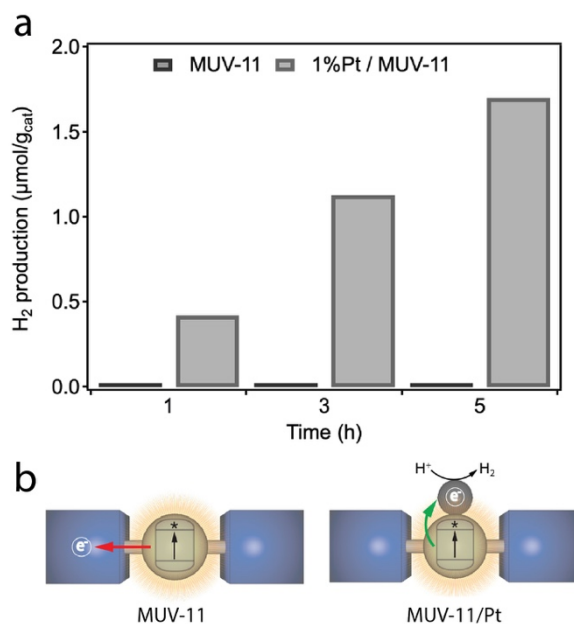

Figure 6. a) Hydrogen production of MUV-11 and 1%Pt-MUV-11 at 1, 3 and 5 hours of illumination with a solar simulator. b) The inactivity of MUV-11 for the HER suggests inefficient charge separation in absence of an applied electrical field (left) that can be overcome by addition of Pt as cocatalyst (right).
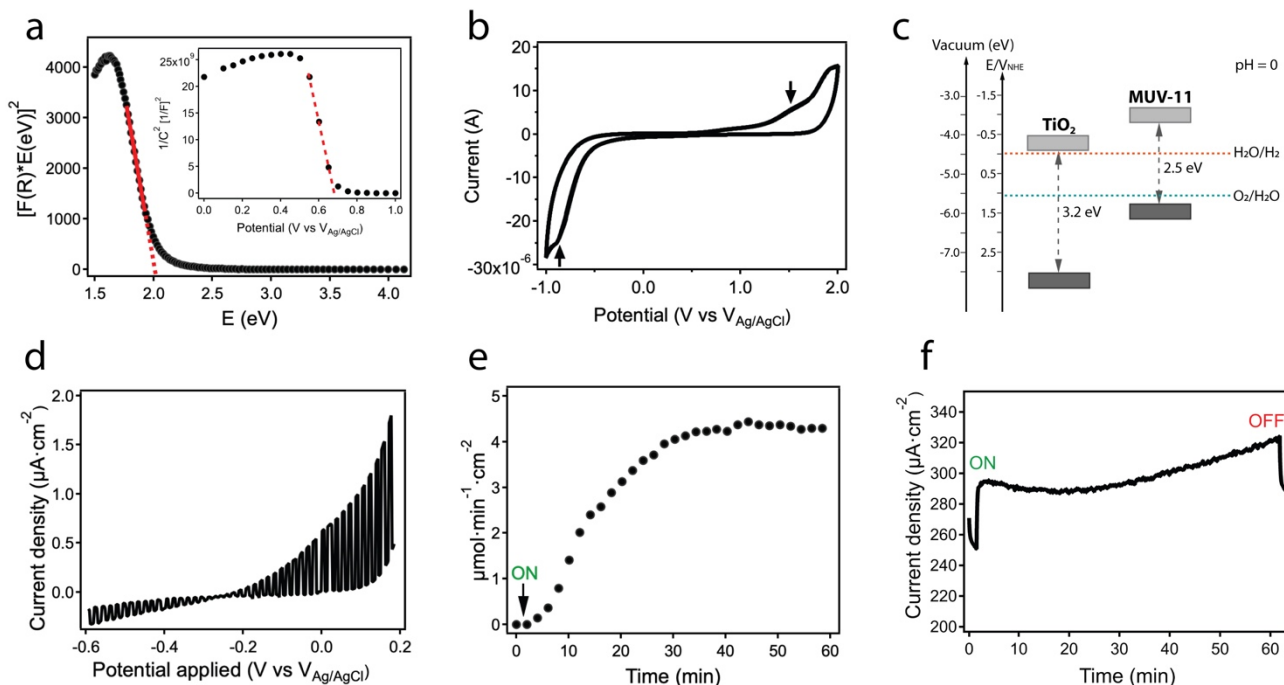
Figure 5. Optical, electrochemical and photoelectrochemical properties of MUV-11. a) Tauc plot of the solid by Kubelka-Munk approximation showing a direct optical band gap of 2.0 eV. Inset: Mott-Schotkky plot at 400Hz with a flat-band potential of 0.68 V. b) Cyclic voltammogram of MUV-11 in nonaqueous electrolyte at 20 mV/sec scan rate. c) Experimental energy diagram showing the alignment of HOMO and LUMO of MUV-11 with the band edges of TiO_2 and the water splitting redox couples at pH = 0. d) Photocurrent density collected under chopped illumination showing the response at different bias potentials. e) Hydrogen evolution under chopped AM 1.5 illumination at 0.5 V vs Ag/AgCl and f) chronoamperometric response recorded simultaneously. See **S7** for experimental details.

principle, MUV-11 would be thermodynamically suitable for photocatalytic water splitting reactions.

We tested the photoelectrochemical activity of MUV-11 films by using the MOF as the working electrode in a three-electrode configuration cell in an argon-purged aqueous electrolyte (0.5 M, Na_2SO_3 in water) with a solar simulator (A. M 1.5) as illumination source. **Figure 5d** shows the chopped-light photocurrent density response at different bias potentials between -0.6 and 0.2 eV *vs* Ag/AgCl, confirming good light absorption for the whole range of potentials studied. Next, we connected the cell to a gas chromatograph and illuminated the films at different bias potentials to evaluate photocatalytic HER. As shown in **Figure 5e**, MUV-11 photoelectrodes display a sigmoidal hydrogen production rate at 0.5V *vs* Ag/AgCl that reaches a plateau after 40 minutes. The experiment was performed for one hour with simultaneous measurement of the photogenerated current. The current density values obtained during the HER remain quite steady, oscillating around 300 ± 20 μA·cm² (**Figure 5f**). We did not observe any signal decay during the experiment that might be indicative of photo-corrosion or passivation of the solid, confirming the excellent stability of MUV-11 in these conditions.

We next tested the activity of the solid without electrical polarization by irradiating a suspension of the solid in H_2O:MeOH (4:1 v/v%) with a solar simulator (**Figure 6**). MUV-11 did not produce measurable amounts of H_2 after 5 hours of irradiation. In turn, after co-deposition of 1% wt. of platinum as co-catalyst, Pt/MUV-11 displayed a linear production of H_2 for a total of 1.7 μmol·g⁻¹ in the same period. No H_2 was produced in the dark confirming the

photocatalytic nature of the reaction. This activity is substantially smaller to that reported for Pt/MIL-125-NH_2 by using TEOA as sacrificial electron donor.[34] PXRD and IR spectra of MUV-11 and Pt/MUV-11 were used to confirm the stability of the material after the photocatalytic experiments (**Figure S32**). Our results confirm the ability of MUV-11 to behave as a hydrogen production photocatalyst but also highlight the necessity of using Pt as a co-catalyst to favour H_2 production in absence of an applied potential acting as driving force. Since the electronic structure of MUV-11 displays appropriate band gap and band edge potentials to tackle this reaction, we decided to

investigate if the photocatalytic efficiency in the hydroxamic MOF might be governed by other parameters.

Effect of the organic connector over photocatalytic activity. We calculated the electronic structure of MUV-11 and other representative photocatalytic Ti-MOFs for a better understanding of the experimental results. **Figure 7a** shows calculated energy levels of MIL-125-NH$_2$, MUV-10(Ca), NTU-9 and MUV-11 and the alignment of the band edges relative to the vacuum level and the potentials of the water oxidation and reduction reactions. The theoretical band gap potentials are consistent with the values reported and confirm that visible-light photoactivity is expected for all MIL-125-NH$_2$ (2.3 eV), MUV-10(Ca) (3.4 eV), NTU-9 (2.0 eV) and MUV-11 (2.1 eV). From a purely thermodynamic point of view, the position of the edge of the lowest unoccupied crystalline orbital (LUCO) relative to the H$_2$O/H$_2$ pair (pH=7, room temperature) is expected to control the turnover for the HER. According to our calculations, the four materials would be thermodynamically suitable for photocatalytic HER with a better performance for NTU-9 and MUV-10(Ca), followed by MIL-125-NH$_2$ and MUV-11 with LUCOs slightly higher in energy. However, this contradicts their experimental performance and the calculated orbital contributions to the LUCO, that are almost exclusively centred in the titanium for MIL-125-NH$_2$ and MUV-10(Ca) whereas electron density is delocalized between Ti and the organic linker orbitals in NTU-9 and MUV-11 (**Figures 7a** and **S35**). Overall, this suggests that the thermodynamic picture is too simple and there must be additional factors governing the photocatalytic performance of MUV-11. We must also consider the kinetics of charge transfer upon illumination.

Efficient charge separation is needed to prevent the fast recombination of the photogenerated charge carriers in order to prolong the lifetime of the excited states.[35] MOFs in which charge separation involves ligand-to-metal charge transfer (LMCT) are arguably more adequate for photocatalytic purposes than others in which the excited state is localized in isolated linkers or metals. Titanium frameworks built from carboxylic acids like terephthalate (MIL-125-NH$_2$) and trimesate (MUV-10(Ca)) undergo LMCT with illumination as confirmed by the presence of photoreduced Ti^{+3} in the electron paramagnetic resonance (EPR) spectra of the irradiated solids.[20,36,37] This behaviour agrees well with their calculated electronic density of states (DOS) diagram (**Figures 7b** and **S34-35**). The highest occupied crystalline orbitals (HOCO) of these frameworks is localized at the organic linker whereas the LUCO is centred on the titanium region. They present a negative ligand-to metal charge-transfer energy (E_{LMCT}), which is defined as the energy change upon transferring an electron from the photoexcited linker orbital to the lower unoccupied metal ion orbital.[38] In turn, MUV-11 and NTU-9, built from hydroxamic and hydroxycarboxylic siderophore metal binders, display LUCOs located simultaneously at the organic linker and the metal. This change in the electronic structure of the frontier orbitals is less likely to induce LMCT for short-lived excitons localized at the organic linker consistent with positive E_{LMCT} values close to zero. The poor photocatalytic performance of MUV-11 seems to be kinetic in origin. Despite its thermodynamic energy alignment is compatible with water reduction, the poor efficiency of LMCT will produce single electron localized photoexcited states, unable to migrate

and reduce the metal nodes for the formation of photocatalytic Ti^{+3} species. Our theoretical findings are consistent with the EPR spectrum of MUV-11 after illumination. We did not observe the occurrence of any paramagnetic signal that could account for the formation of photogenerated Ti^{3+} species (**Figure S33**). These results are
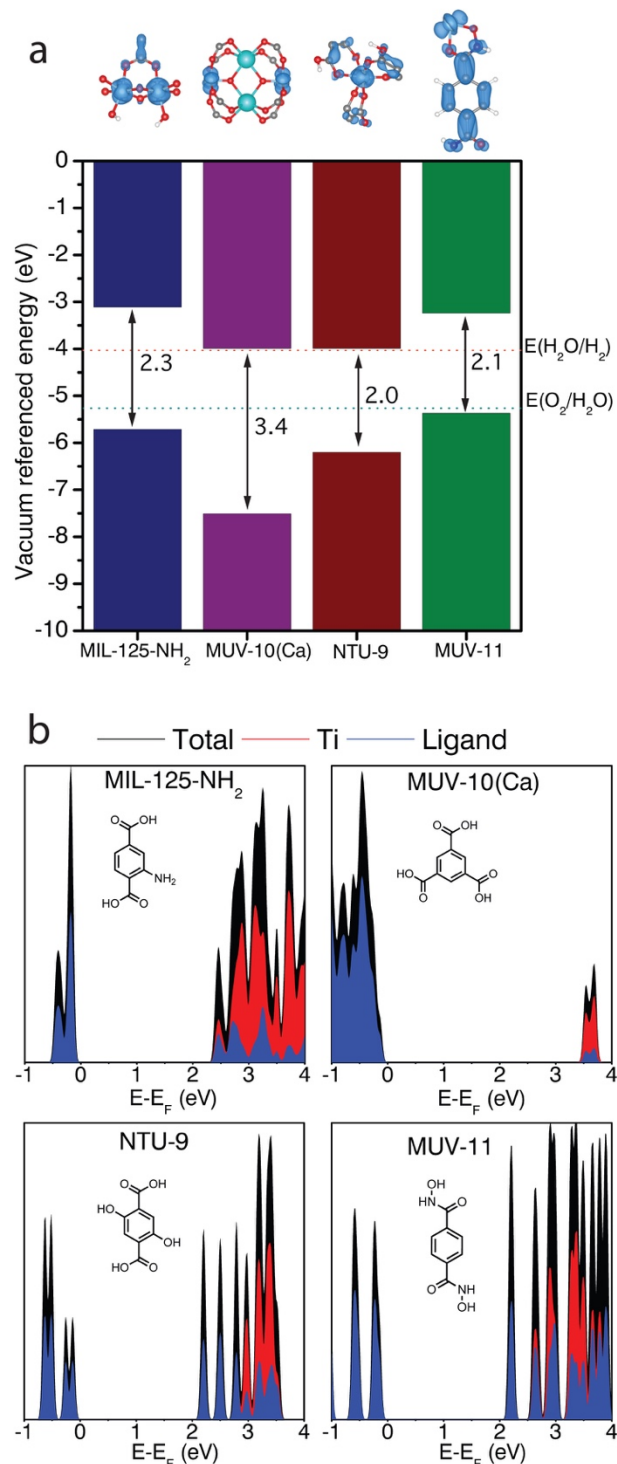

Figure 7. a) Electronic band alignment relative to the vacuum level and the water oxidation/reduction potentials at pH=7 (dot lines) for selected Ti-MOFs. Orbitals contributing to LUCO (top). b) Total (black) and projected (Ti in red and ligand in blue) density of states for MIL-125-NH2, MUV-10(Ca), NTU-9 and MUV-11.

consistent with recent reports,[39,40] that highlight the importance of orbital contributions at the band edges in controlling LMCT and thereby the photocatalytic efficiency of UiO-type MOFs with the introduction of different d^0 metals (Ti, Zr, Hf, Ce, Th or U). Our results suggest that not only to the unoccupied bands of the metallic nodes but also the metal binding group and the chemistry of this particular type of linkers can introduce changes to the electronic structure of the frontier orbitals in these solids also relevant to their function

CONCLUSIONS

The design of chemically stable MOFs, and more particularly titanium-organic frameworks, is still restricted to a limited group of metal connectors. We report for the first time the ability of hydroxamic acids to produce reticular solids by *de novo* synthesis. MUV-11 is a crystalline, porous material that combines photo-activity with outstanding chemical stability in acid conditions intrinsic to the introduction of siderophore metal binders. Compared to other carboxylate Ti frameworks, this hydroxamate MOF can be prepared as single crystalline phases for multiple titanium salts, thus expanding the scope of precursors accessible to this chemistry. We make use of photoelectrochemical and catalytic studies to compare the electronic structure and photoactivity of MUV-11 with other selected materials like MIL-125-NH$_2$, MUV-10(Ca) and NTU-9. Computational modelling reveals striking differences in the charge separation kinetics of the MOFs built from siderophores. These are less likely to undergo photo-stimulated LMCT for generating active Ti^{+3} species as result of the delocalization of the electronic density delocalized between the metal node and the organic linker. Provided the principles of isoreticular chemistry, the straightforward derivatization of carboxylic linkers with hydroxamic groups might represent an alternative synthetic platform for the synthesis of crystalline titanium MOFs. We hope this combination of experiment and theory will help delineate future directions in this context.

We are confident this work might as well offer new perspectives for the chemistry of Covalent Organic Frameworks (COFs). The critical step in the crystallization of COFs is to reach synthetic conditions that enable reversible formation of covalent bonds between building blocks to enable defect repair during crystal growth.[41,42] Either by direct condensation or controlled hydrolysis of hydroxamic acid connectors into carboxylic acids, these linkers might help gaining control over covalent bond formation and inspire similar approaches to grow COF crystals.

EXPERIMENTAL SECTION

Synthesis of MUV-11. H$_4$bdha (70.6 mg; 0.36 mmol) was suspended in a mixture of 7.2 mL of *N,N*-dimethylformamide and 2.1 mL of AcOH in a 25 mL Schott bottle. Subsequently, 72 µmol of the titanium precursor were added to the suspension. The bottle was sealed and heated in an oven at 120 ºC for 48 hours. After cooling down to room temperature, this results in the formation of hexagonal orange crystals that were isolated by filtration and rinsed with 45 mL of DMF (3x15 mL) and 45 mL of acetone (3x15 mL). The product was dried at room temperature.

Photoelectrochemical measurements. Experiments were performed in a three-electrode glass cell with a quartz window containing an aqueous solution of 0.5M. MUV-11 powders suspensions were deposited by drop casting on ITO cover glasses and used as working electrode. The counter electrode was a platinum wire, and the reference one was an Ag/AgCl electrode. Voltage, current density (at dark and under illumination) and electrochemical impedance spectroscopy were measured with a potentiostat-galvanostat PGSTAT204 provided with an integrated impedance module FRAII (10 mV of modulation amplitude is used at 400Hz). A solar Simulator (LOT LSH302 Xe lamp and a LSZ389 AM1.5 Global filter) was used as a light source.

Photocatalytic experiments. The photocatalytic activity of MUV-11 for H$_2$ evolution was performed by irradiating a dispersion of 1 mg/ml of the MOF in H$_2$O:MeOH solutions (4:1 v/v%) in sealed vessels, purged with Ar. As-made MUV-11 was activated in vacuum before purging with N$_2$, in some cases 1% wt. Pt was photodeposited in the solution. The suspension was kept under constant stirring and irradiated with a solar simulator (253 W) at room temperature. The formation of gases in the liquid phase was detected with a PerkinElmer (Clarus 580GC) gas chromatograph equipped with a TCD detector.

Computational details. All calculations were performed with periodic density functional theory by using the Vienna ab initio Simulation package (VASP).[43,44] For the geometry optimizations, we used the generalized gradient approximation (GGA) with the Perdew–Burke–Ernzerhof (PBE) functional,[45] and including van der Waals (vdW) corrections via the DFT-D3 method of Grimme.[46,47] The kinetic energy cut-off for the plane-wave basis set expansion was chosen as 500 eV, and a Γ-points were used for integrations in the reciprocal space, due to the large size of the unit cell of the direct lattice. Finally, the total density of states (DOS) and the electronic band structure of the crystalline solids were calculated by using the screened hybrid functional of Heyd, Scuseria and Ernzerhof (HSE06).[48] The electron energies were aligned to the vacuum level using a procedure reported by Butler and co-workers.[49]

ASSOCIATED CONTENT

AUTHOR INFORMATION

Corresponding Author

* E-mail: carlos.marti@uv.es

Present Addresses

† Department of Chemistry, Scripps Research, 10550 North Torrey Pines Road, La Jolla, CA 92037, (United States).

Author Contributions

The manuscript was written through contributions of all authors. All authors have given approval to the final version of the manuscript.
‡ These authors contributed equally.

REFERENCES

(1) Furukawa, H.; Cordova, K. E.; O'Keeffe, M.; Yaghi, O. M. The Chemistry and Applications of Metal-Organic Frameworks. *Science* **2013**, *341* (6149), 1230444.

(2) Colombo, V.; Galli, S.; Choi, H.; Han, G.; Maspero, A.; Palmisano, G.; Masciocchi, N.; Long, J. R. High Thermal and Chemical Stability in Pyrazolate-Bridged Metal–Organic Frameworks with Exposed Metal Sites. *Chem. Sci.* **2011**, *2* (7), 1311.

(3) Park, K.; Ni, Z.; Côté, A.; Choi, J.; Huang, R.; Uribe-Romo, F.; Chae, H.; O'Keeffe, M.; Yaghi, O. M. Exceptional Chemical and Thermal Stability of Zeolitic Imidazolate Frameworks. *Proc. National Acad. Sci.* **2006**, *103* (27), 10186.

(4) Serre, C.; Millange, F.; Thouvenot, C.; Noguès, M.; Marsolier, G.; Louër, D.; Ferey, G. Very Large Breathing Effect in the First Nanoporous Chromium(III)-Based Solids: MIL-53 or CrIII(OH)·{O$_2$C-C$_6$H$_4$- CO$_2$}·{HO$_2$C-C$_6$H$_4$-CO$_2$H}x·H$_2$O$_y$. *J. Am. Chem. Soc.* **2002**, *124* (45), 13519-13526.

(5) Ferey, G.; Serre, C.; Mellot-Draznieks, C.; Millange, F.; Surblé, S.; Dutour, J.; Margiolaki, I. A Hybrid Solid with Giant Pores Prepared by a Combination of Targeted Chemistry, Simulation, and Powder Diffraction. *Angew. Chem. Int. Ed.* **2004**, *43* (46), 6296-6301.

(6) Ferey, G.; Mellot-Draznieks, C.; Serre, C.; Millange, F.; Dutour, J.; Surblé, S.; Margiolaki, I. A Chromium Terephthalate-Based Solid with Unusually Large Pore Volumes and Surface Area. *Science* **2005**, *309* (5743), 2040-2042.

(7) Cavka, J.; Jakobsen, S.; Olsbye, U.; Guillou, N.; Lamberti, C.; Bordiga, S.; Lillerud, K. A New Zirconium Inorganic Building Brick Forming Metal Organic Frameworks with Exceptional Stability. *J. Am. Chem. Soc.* **2008**, *130* (42), 13850-13851.

(8) Devic, T.; Serre, C. High Valence 3p and Transition Metal Based MOFs. *Chem. Soc. Rev.* **2014**, *43* (16), 6097-6115.

(9) Bai, Y.; Dou, Y.; Xie, L.-H.; Rutledge, W.; Li, J.-R.; Zhou, H.-C. Zr-Based Metal-Organic Frameworks: Design, Synthesis, Structure, and Applications. *Chem. Soc. Rev.* **2016**, *45* (8), 2327-2367.

(10) Howarth, A. J.; Liu, Y.; Li, P.; Li, Z.; Wang, T. C.; Hupp, J. T.; Farha, O. K. Chemical, Thermal and Mechanical Stabilities of Metal-Organic Frameworks. *Nat. Rev. Mater.* **2016**, *1* (3), 15018.

(11) Yuan, S.; Qin, J.-S.; Lollar, C. T.; Zhou, H.-C. Stable Metal–Organic Frameworks with Group 4 Metals: Current Status and Trends. *ACS Cent. Sci* **2018**, *4* (4), 440-450.

(12) Assi, H.; Mouchaham, G.; Steunou, N.; Devic, T.; Serre, C. Titanium Coordination Compounds: From Discrete Metal Complexes to Metal-Organic Frameworks. *Chem. Soc. Rev.* **2017**, *46* (11), 3431-3452.

(13) Dan-Hardi, M.; Serre, C.; Frot, T.; Rozes, L.; Maurin, G.; Sanchez, C.; Ferey, G. A New Photoactive Crystalline Highly Porous Titanium (IV) Dicarboxylate. *J. Am. Chem. Soc.* **2009**, *131* (31), 10857-10859.

(14) Yuan, S.; Liu, T.-F.; Feng, D.; Tian, J.; Wang, K.; junsheng qin; Zhang, Q.; Chen, Y.-P.; Bosch, M.; Zou, L.; et al. A Single Crystalline Porphyrinic Titanium Metal-Organic Framework. *Chem. Sci.* **2015**, *6* (7), 3926-3930.

(15) Mason, J. A.; Darago, L. E.; Jr., W. W.; Long, J. R. Synthesis and O$_2$ Reactivity of a Titanium(III) Metal–Organic Framework. *Inorg. Chem.* **2015**, *54* (20), 10096-10104.

(16) Nguyen, H. L.; Gándara, F.; Furukawa, H.; Doan, T. L.; Cordova, K. E.; Yaghi, O. M. A Titanium−Organic Framework as an Exemplar of Combining the Chemistry of Metal– and Covalent−Organic Frameworks. *J. Am. Chem. Soc.* **2016**, *138* (13), 4330-4333.

(17) Wang, C.; Liu, C.; He, X.; Sun, Z.-M. A Cluster-Based Mesoporous Ti-MOF with Sodalite Supercages. *Chem. Commun.* **2017**, *53* (85), 11670-11673.

(18) Yuan, S.; Qin, J.-S.; Xu, H.-Q.; Su, J.; Rossi, D.; Chen, Y.; Zhang, L.; Lollar, C.; Wang, Q.; Jiang, H.-L.; et al. [Ti$_8$Zr$_2$O$_{12}$(COO)$_{16}$] Cluster: An Ideal Inorganic Building Unit for Photoactive Metal–Organic Frameworks. *ACS Cent. Sci.* **2017**, *4* (1), 105-111.

(19) Wang, S.; Kitao, T.; Guillou, N.; Wahiduzzaman, M.; Martineau-Corcos, C.; Nouar, F.; Tissot, A.; Binet, L.; Ramsahye, N.; Devautour-Vinot, S.; et al. A Phase Transformable Ultrastable Titanium-Carboxylate Framework for Photoconduction. *Nat. Commun.* **2018**, *9* (1), 1660.

(20) Castells-Gil, J.; M. Padial, N.; Almora-Barrios, N.; Albero, J.; Ruiz-Salvador, R. A.; González-Platas, J.; García, H.; Martí-Gastaldo, C. Chemical Engineering of Photoactivity in Heterometallic Titanium–Organic Frameworks by Metal Doping. *Angew. Chem. Int. Ed.* **2018**, *57* (28), 8453–8457.

(21) Keum, Y.; Park, S.; Chen, Y.-P.; Park, J. Titanium-Carboxylate Metal-Organic Framework Based on an Unprecedented Ti-Oxo Chain Cluster. *Angew. Chem. Int. Ed.* **2018**, *57* (45), 14852-14856.

(22) Castells-Gil, J.; M. Padial, N.; Almora-Barrios, N.; da Silva, I.; Mateo, D.; Albero, J.; Garcia, H.; Martí-Gastaldo, C. De Novo Synthesis of Mesoporous Photoactive Titanium(IV)-Organic Frameworks with MIL-100 Topology. *Chem. Sci.* **2019**, *10* (15), 4313-4321.

(23) Nguyen, N. T.; Furukawa, H.; Gándara, F.; Trickett, C. A.; Jeong, H.; Cordova, K. E.; Yaghi, O. M. Three-Dimensional Metal-Catecholate Frameworks and Their Ultrahigh Proton Conductivity. *J. Am. Chem. Soc.* **2015**, *137* (49), 15394-15397.

(24) Gao, J.; Miao, J.; Li, P.-Z.; Teng, W.; Yang, L.; Zhao, Y.; Liu, B.; Zhang, Q. A P-Type Ti(IV)-Based Metal–Organic Framework with Visible-Light Photo-Response. *Chem. Commun.* **2014**, *50* (29), 3786-3788.

(25) Assi, H.; Pérez, L. C.; Mouchaham, G.; Ragon, F.; Nasalevich, M.; Guillou, N.; Martineau, C.; Chevreau, H.; Kapteijn, F.; Gascon, J.; et al. Investigating the Case of Titanium(IV) Carboxyphenolate Photoactive Coordination Polymers. *Inorg. Chem.* **2016**, *55* (15), 7192-7199.

(26) Marmion, C. J.; Griffith, D.; Nolan, K. B. Hydroxamic Acids – An Intriguing Family of Enzyme Inhibitors and Biomedical Ligands. *Eur. J. Inorg. Chem.* **2004**, 15, 3003–3016.

(27) Pereira, C. F.; Howarth, A. J.; Vermeulen, N. A.; Paz, F. A.; Tomé, J. P.; Hupp, J. T.; Farha, O. K. Towards Hydroxamic Acid Linked Zirconium Metal−Organic Frameworks. *Mater. Chem. Front.* **2017**, *1* (6), 1194-1199.

(28) Griffith, D.; Krot, K.; Comiskey, J.; Nolan, K. B.; Marmion, C. J. Monohydroxamic Acids and Bridging Dihydroxamic Acids as Chelators to Ruthenium(III) and as Nitric Oxide Donors : Syntheses, Speciation Studies and Nitric Oxide Releasing Investigation. *Dalton Trans.* **2007**, 1, 137–147.

(29) Gao, W.-Y.; Wojtas, L.; Ma, S. A Porous Metal–Metalloporphyrin Framework Featuring High-Density Active Sites for Chemical Fixation of CO$_2$ under Ambient Conditions. *Chem. Commun.* **2014**, *50* (40), 5316-5318.

(30) Bueken, B.; Vermoortele, F.; Vanpoucke, D. E.; Reinsch, H.; Tsou, C.-C.; Valvekens, P.; Baerdemaeker, T.; Ameloot, R.; Kirschhock, C. E.; Speybroeck, V.; et al. A Flexible Photoactive Titanium Metal-Organic Framework Based on a [Ti(IV)$_3$(μ_3-O)(O)$_2$(COO)$_6$] Cluster. *Angew. Chem. Int. Ed.* **2015**, *54* (47), 13912-13917.

(31) Schubert, U. Chemical Modification of Titanium Alkoxides for Sol–Gel Processing. *J. Mater. Chem.* **2005**, *15* (35–36), 3701-3715.

(32) Ahmed, E.; Holmström, S. Siderophores in Environmental Research: Roles and Applications. *Microb. Biotechnol.* **2014**, *7* (3), 196-208.

(33) Dhakshinamoorthy, A.; Asiri, A. M.; García, H. Metal-Organic Framework (MOF) Compounds: Photocatalysts for Redox Reactions and Solar Fuel Production. *Angew. Chem. Int. Ed.* **2016**, *55* (18), 5414-5445.

(34) Horiuchi, Y.; Toyao, T.; Saito, M.; Mochizuki, K.; Iwata, M.; Higashimura, H.; Anpo, M.; Matsuoka, M. Visible-Light-Promoted Photocatalytic Hydrogen Production by Using an Amino-Functionalized Ti(IV) Metal–Organic Framework. *J. Phys.Chem. C* **2012**, *116* (39), 20848-20853.

(35) Allendorf, M.; Bauer, C.; Bhakta, R.; Houk, R. Luminescent Metal–Organic Frameworks. *Chem. Soc. Rev.* **2009**, *38* (5), 1330−1352.

(36) Nasalevich, M.; Becker, R.; Ramos-Fernandez, E.; Castellanos, S.; Veber, S.; Fedin, M.; Kapteijn, F.; Reek, J.; van der Vlugt, J.; Gascón, J. Co@NH_2-MIL-125(Ti): Cobaloxime-Derived Metal–Organic Framework-Based Composite for Light-Driven H_2 Production. *Energy Env. Sci.* **2015**, *8* (1), 364-375.

(37) Chambers, M. B.; Wang, X.; Ellezam, L.; Ersen, O.; Fontecave, M.; Sanchez, C.; Rozes, L.; Mellot-Draznieks, C. Maximizing the Photocatalytic Activity of Metal–Organic Frameworks with Aminated-Functionalized Linkers: Substoichiometric Effects in MIL-125-NH_2. *J. Am. Chem. Soc.* **2017**, *139* (24), 8222-8228.

(38) Vos, A.; Hendrickx, K.; Voort, P.; Speybroeck, V.; Lejaeghere, K. Missing Linkers: An Alternative Pathway to UiO-66 Electronic Structure Engineering. *Chem. Mater.* **2017**, *29* (7), 3006-3019.

(39) Nasalevich, M. A.; Hendon, C. H.; Santaclara, J. G.; Svane, K.; van der Linden, B.; Veber, S. L.; Fedin, M. V.; Houtepen, A. J.; van der Veen, M. A.; Kapteijn, F.; et al. Electronic Origins of Photocatalytic Activity in d⁰ Metal Organic Frameworks. *Sci. Rep.* **2016**, *6* (1), 23676.

(40) Wu, X.-P.; Gagliardi, L.; Truhlar, D. G. Cerium Metal–Organic Framework for Photocatalysis. *J. Am. Chem. Soc.* **2018**, *140* (25), 7904-7912.

(41) Ma, T.; Kapustin, E. A.; Yin, S. X.; Liang, L.; Zhou, Z.; Niu, J.; Li, L.-H.; Wang, Y.; Su, J.; Li, J.; et al. Single-Crystal x-Ray Diffraction Structures of Covalent Organic Frameworks. *Science* **2018**, *361* (6397), 48-52.

(42) Navarro, J. A. R. The Dynamic Art of Growing COF Crystals. *Science* **2018**, *361* (6397), 35.

(43) Kresse, G.; Furthmüller, J. Efficiency of Ab-Initio Total Energy Calculations for Metals and Semiconductors Using a Plane-Wave Basis Set. *Comput. Mater. Sci.* **1996**, *6* (1), 15-50.

(44) Kresse, G.; Furthmüller, J. Efficient Iterative Schemes for Ab Initio Total-Energy Calculations Using a Plane-Wave Basis Set. *Phys. Rev. B* **1996**, *54* (16), 11169-11186.

(45) Perdew, J. P.; Burke, K.; Ernzerhof, M. Generalized Gradient Approximation Made Simple. *Phys. Rev. Lett.* **1996**, *77* (18), 3865-3868.

(46) Grimme, S.; Antony, J.; Ehrlich, S.; Krieg, H. A Consistent and Accurate Ab Initio Parametrization of Density Functional Dispersion Correction (DFT-D) for the 94 Elements H-Pu. *J. Chem. Phys.* **2010**, *132* (15), 154104.

(47) Bučko, T.; Hafner, J.; Lebègue, S.; Ángyán, J. G. Improved Description of the Structure of Molecular and Layered Crystals: Ab Initio DFT Calculations with van Der Waals Corrections. *J. Phys. Chem. A* **2010**, *114* (43), 11814-11824.

(48) Heyd, J.; Scuseria, G. E.; Ernzerhof, M. Hybrid Functionals Based on a Screened Coulomb Potential. *J. Chem. Phys.* **2003**, *118* (18), 8207-8215.

(49) Butler, K. T.; Hendon, C. H.; Walsh, A. Electronic Chemical Potentials of Porous Metal–Organic Frameworks. *J. Am. Chem. Soc.* **2014**, *136* (7), 2703–2706.